Controllable preparation and photocatalytic activity of highly ordered ZnO nanoarrays

Xia Kong[1], *Yawei Hu*[1] ✉, *Wei Pan*[2]

[1]*College of Chemistry and Chemical Engineering, Shaanxi University of Science and Technology, Xi'an, Shaanxi 710021, People's Republic of China*
[2]*State Key Laboratory of New Ceramics and Fine Processing, Tsinghua University, Beijing 100084, People's Republic of China*
✉ *E-mail: huyawei@sina.com*

Published in Micro & Nano Letters; Received on 16th January 2017; Revised on 23rd February 2017; Accepted on 10th March 2017

Well-aligned ZnO nanotubular arrays (NTs) and nano rod-like arrays (NRs) were controllably fabricated on glass substrates through a facile hydrothermal method, and the prepared ZnO nanoarrays could be easily retrieved in the photodegradation of organic pollutants because ZnO is "growing" on the substrates. The morphology of ZnO nanoarrays could be governed by the cooling process and reaction time during the preparation. ZnO NTs tend to be formed by natural cooling, while ZnO NRs are apt to be constructed by sudden cooling. Furthermore, with the proceeding of the reaction, the ZnO nanoarrays display headless-pyramid configuration gradually. The ZnO nanoarrays prepared at 90 ºC for 4 h show excellent photocatalytic activity. In the presence of the prepared ZnO NTs and NRs, the degradation rate of methylene blue (MB) is up to 96.8% and 94.1% after 1 h UV irradiation, respectively. The better photocatalytic performance of ZnO NTs is ascribed to the highly ordered array and large specific surface area which could promote the transfer of photo-generated electrons and restrain the recombination of electron-hole pairs. The well-aligned ZnO nanoarrays in this study could be fabricated on different substrates. Moreover, they could potentially serve as excellent photocatalysts in waste water treatment.

1. Introduction: In recent years, environmental pollution and energy shortage have become two major global issues. Semiconductor oxide photocatalytic materials with great application prospect in resolving these two issues attract extensive attention in the world [1–3]. Photocatalysis, as a kind of 'green technology' to degrade the organic matter by photocatalytic oxidation reaction, open a new door for the elimination of organic pollutants in wastewater [1, 4, 5]. Up to date, ZnO has been regarded as an excellent photocatalytic material due to its high photosensitivity, non-toxic nature, non-secondary pollution and low selectivity of pollutants [6–10]. Especially, the interest in the fabrication of one-dimensional ZnO nanoarrays, such as nanowires [11], nanoneedles [12], nanorods [13] and nanotubes [14], is driven because of their exceptional properties and potential applications in elimination of environment pollutants.

However, when ZnO is employed as the photocatalyst for organic pollutant degradation, three aspects should be considered: (i) although the photocatalytic property of ZnO nanoparticles has been reported in lots of literature, there are still many disadvantages for these nanoparticles, such as aggregation, deactivation and non-recycle, which limit their application in photocatalytic technology [15]; (ii) ZnO is a wide bandgap II–VI compound with 3.37 eV direct bandgap and 60 meV free-exciton excitation energy at room temperature. Therefore, the band edge absorption threshold does not allow the utilisation of visible light [16]; (iii) the electron transfer step plays a vital role in the degradation of dyes. It has been found that the fast recombination of photoexcited electrons and holes in semiconductor adversely affects the photocatalytic efficiency [17]. Taking the above three aspects into account, how to set up a stable photocatalytic system with high catalytic efficiency, rapid responsibility to visible light, pollution-free, as well as easily retrievable characteristics will be of great importance.

It is reported that highly ordered arrays could lead to a remarkable decrease in the e^-/h^+ recombination [18] compared with the random nanostructures, which will result in the enhancement of photocatalytic activity. ZnO NTs with a larger specific surface area and high adsorption capacity, are expected to display a high photocatalytic activity. Furthermore, the ZnO NTs growing on substrates could be retrieved easily, which will extend their applications. Therefore, ZnO nanoarrays on different substrates, especially ZnO nanotubular arrays, become a kind of promising photocatalytic materials. Up to now, the principal techniques used for growing ZnO nanoarrays include template-assisted growth [19], noble metal catalytic growth [20], chemical and physical vapour deposition [21], sol–gel method [22] and hydrothermal method [23]. Among these techniques, hydrothermal synthesis is a simple and effective means to prepare nanoarrays on substrates. In this Letter, the well-aligned ZnO NTs and NRs on indium tin oxide (ITO) substrate are controllably fabricated at a relatively low temperature (90°C), and their photocatalytic performances have been evaluated as well.

2. Experimental method: All reagents were of analytical grade and used without further purification in this work. ITO glasses (3.5 × 2 cm) were used as substrates.

Prior to use, ITO glasses were ultrasonically cleaned in acetone, isopropyl alcohol, ethanol and distilled water for 15 min, respectively, and then were washed with deionised water three times to remove any residual solution and dried under nitrogen flow.

2.1. Preparation of ZnO seed membrane: As a typical procedure, 0.1 g polyvinylpyrrolidone was dissolved in absolute ethanol (8 ml) with magnetic stirring for 1 h. The obtained solution was dropwise added to zinc nitrate hexahydrate solution ($Zn(NO_3)_2{\cdot}6H_2O$, 2.98 g in 2 ml deionised water) with continuous stirring for 8–10 h. Then, the solution was placed at room temperature more than 48 h to form ZnO seed solution. ZnO seed membrane was fabricated on clean substrates by dip-coating method, followed by annealing at 400°C for 1 h in air.

2.2. Growth of ZnO nanoarrays: The growth of ZnO nanoarrays was carried out by immersing the nanoseeds-attached substrates

into equimolar (50 mmol l^{-1}) solution of $Zn(NO_3)_2$ and hexamethyl-enetetramine (HMT). The growth solutions were transferred and sealed in Teflon-lined stainless steel autoclaves of 20 ml, in which the substrates with ZnO seed layers were vertically placed. The autoclaves were heated to 90°C with a heating rate of 1°C min^{-1} and kept for different time, followed by cooling the autoclaves down to room temperature naturally and suddenly, respectively. Then, the obtained ZnO nanoarrays were thoroughly rinsed with distilled water and dried in air. Based on this, ZnO NTs obtained under 90°C for 4 h with natural and sudden cooling way were labelled as ZnO NTs-4-N and ZnO NRs-4-S, respectively. Accordingly, ZnO NTs obtained under 90°C for 8 h with natural and sudden cooling way were named as ZnO NTs-8-N and ZnO NRs-8-S, respectively.

2.3. Characterisation: X-ray diffraction (XRD) was carried out using a Rigaku-Ultima IV diffractometer with Cu-K_α radiation ($\lambda = 0.15405$ nm) at a scanning speed of 8° min^{-1} ranging from 20° to 80°. The morphologies of ZnO nanoarrays were characterised by a Rigaku-S4800 scanning electron microscope (SEM, Tokyo, Japan). UV–visible diffuse reflectance spectra were recorded with an America Agilent Cary 5000 spectrophotometer range from 200 to 800 nm. The photoluminescence (PL) spectra were performed using a FluoroMax-4P fluorescence phosphorescence thermoluminescence spectrometer (Horiba, Japan).

The electrochemical impedance spectra (EIS) measurements were carried out on a Parstat Mc electrochemical workstation (Ametek Company, America) by using three-electrode system. The quartz electrolytic cell was filled with 0.1 mol l^{-1} Na_2SO_4 electrolyte. An CLS-002 UV lamp (8 W, the strongest emission at 254 nm) was used as the light source. The ZnO nanoarrays grown on ITO glasses were used as working electrodes. The counter and reference electrodes were a platinum sheet and saturated calomel electrode, respectively. The impedance spectra were recorded over the frequency range of 0.05–10^5 Hz.

The photocatalytic activities of ZnO NTs-4-N and ZnO NRs-4-S were evaluated by the degradation of methylene blue (MB) solution, which is usually used to investigate photocatalytic activities [4, 5, 15, 24], by using a 500 W mercury lamp in an annular type UV photoreactor (Bilong Biological Technology Company Ltd, Xi'an, China). Prior to ultraviolet irradiation, the samples were immersed in 20 ml MB solution (4 mg l^{-1}), and then the solution was magnetically stirred in dark for 30 min to ensure an establishment of an adsorption–desorption equilibrium of MB. The degradation of MB solution was monitored by a Hach-Dr 5000 UV–visible spectrophotometer periodically and the absorption of the MB solution at 664 nm was recorded as a function of irritation time.

3. Results and discussion: First, the growth mechanism of prepared ZnO nanoarrays is investigated. The formation of ZnO crystal seed mainly comprises two steps: nucleation and growth. Seed-mediated synthesis of ZnO not only provides homogeneous nucleation centre, but induces the growth of nanoarrays to be well ordered, more closely arranged and vertical to the substrate [25]. In the process of growth, $Zn(NO_3)_2$ and HMT are used as sources of zinc ion (Zn^{2+}) and hydroxide ions (OH), respectively. With the increase of growth temperature, ammonia generates from the decomposition of HMT and $Zn(OH)_2$ occurs. As the proceeding of the reaction and the further increase of the reaction temperature, more ZnO nuclei form on the substrate, and gradually ZnO film grows from the nuclei. The chemical reaction can be represented as follows

$$(CH_2)_6N_4 + 6H_2O \rightarrow 6HCHO + NH_3 \quad (1)$$

$$NH_3 + H_2O \leftrightarrow NH_4^+ + OH^- \quad (2)$$

$$2OH^- + Zn^{2+} \rightarrow Zn(OH)_2 \quad (3)$$

$$Zn(OH)_2 \rightarrow ZnO(s) + H_2O \quad (4)$$

$$ZnO + 2OH^- \rightarrow ZnO_2^{2-} + H_2O \quad (5)$$

At first, the reaction is positive and can continuously form ZnO nanorod arrays (4). However, with the gradual decrease of the reactants concentration, the dissolution effect of the reaction gradually dominates and the generated ZnO is dissolved slowly (5) [26, 27]. ZnO, as a polar crystal, is divided into polar surface and non-polar surface. On the tops of the nanorods, (0001) plane is a polar surface with higher surface energy that is more easily dissolved. When the reaction time is prolonged, the polar surface (0001) dissolves quickly in the *c*-axis and continuously erodes to form the nanotubes [27].

Fig. 1 shows the SEM of ZnO NTs and NRs. Figs. 1*a* and *b* are the ZnO NTs-4-N images, which display that ZnO NTs were successfully fabricated and vertically grown on the substrate under 90°C for 4 h with natural cooling, and the average outer diameter is about 125 nm and inner diameter is about 100 nm. Figs. 1*c* and *d* are the images of ZnO NRs-4-S obtained under 90°C for 4 h with sudden cooling after heating completed, which indicates that the sudden cooling results in ZnO NRs. The average diameter of ZnO NRs-4-S is about 120 nm.

Fig. 2 shows the morphologies of ZnO NTs-8-N and ZnO NRs-8-S which were prepared at 90°C for 8 h with natural cooling way and sudden cooling way, respectively. It can be seen

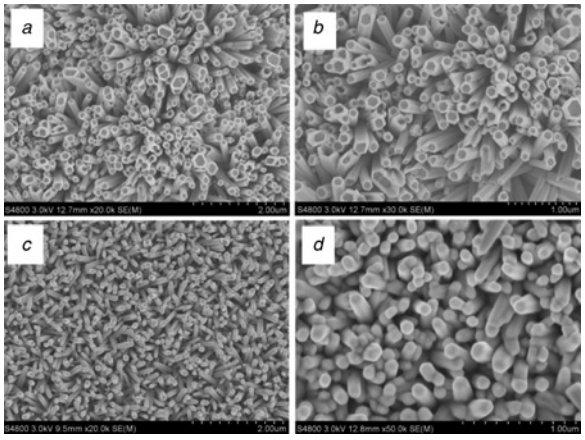

Fig. 1 *SEM images of*
a and *b* ZnO NTs-4-N
c and *d* ZnO NRs-4-S

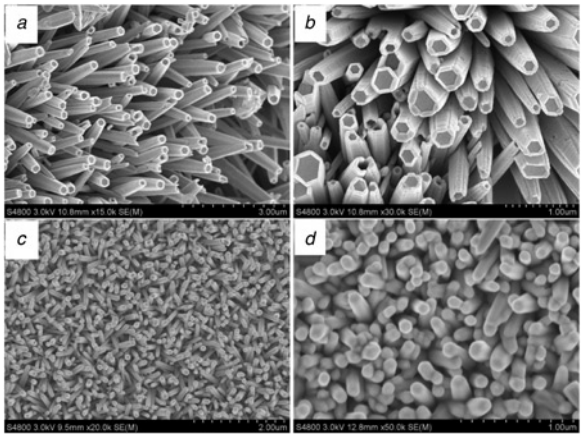

Fig. 2 *SEM images of*
a and *b* ZnO NTs-8-N
c and *d* ZnO NRs-8-S

doi: 10.1049/mnl.2016.0819

from Figs. 2*a* and *b* that average outer diameter of ZnO NTs-8-N is about 250 nm, and the inner diameter is about 160 nm. On the contrary, the average diameter of ZnO NRs-8-S, which were obtained with sudden cooling, is about 140 nm (Figs. 2*c* and *d*).

Compared with ZnO nanotubes and nanorods prepared at 90°C for 4 h, ZnO nanoarrays, either ZnO NTs-8-N or ZnO NRs-8-S obtained at 90°C for 8 h, display headless-pyramid configuration, which might be attributed to the decrease of Zn^{2+} concentration in solution with the reaction proceeding and ZnO growing.

Furthermore, ZnO NTs could be obtained when the autoclaves were cooled naturally, such as ZnO NTs-4-N and ZnO NTs-8-N. However, ZnO NRs were achieved with sudden cooling, like as ZnO NRs-4-S and ZnO NRs-8-S. When the reaction temperature decreases suddenly, the potential kinetic energy of Zn^{2+} and OH forming ZnO crystals becomes weak in solution. Meanwhile, the decomposition of HMT stops and no ammonia generates which leads to the decrease of OH^- concentration in solution. The generation of ZnO is restrained based on (3) and (4). Simultaneously, according to (5) and the description in growth mechanism, the ZnO NTs could not be formed through the dissolution of the polar surface (0001) of ZnO crystal. It is also suggested that the precursor solutions with lower concentration of OH^- ions are not able to produce ZnO NTs via selective self-etching at low temperature [28].

The XRD patterns of ZnO NTs-4-N and ZnO NRs-4-S are shown in Fig. 3. It is found that both samples present the typical XRD diffraction character of wurtzite structure of ZnO, which are in good agreement with the standard card (JCPDS Card No. 36-1451). No other diffraction peaks are found, which demonstrates that the products are pure. The intensity of (002) peak is the strongest and sharpest in all of the peaks, which indicates there is a strong preferred growth orientation along the *c*-axis [29]. It is also noted that the (002) peaks of NTs and NRs arrays are account for dominant position. However, the strength of the former is weaker than that of the latter obviously, which is due to the apical dissolution of nanotube (002) crystal plane. The XRD results are consistent with the growth mechanism of ZnO arrays.

The photocatalytic activities of ZnO NTs-4-N and ZnO NRs-4-S were investigated through monitoring the concentration of MB solution within 60 min under UV light irradiation. The result is shown in Fig. 4. It is found that the MB solution is nearly not degraded under UV irradiation in the absence of ZnO catalysts (Fig. 4*a*). However, the presence of the synthesised ZnO NTs-4-N and ZnO NRs-4-S accelerates MB degradation greatly and the degradation results are shown in Figs. 4*b* and *c*. Obviously, ZnO NTs-4-N exhibits higher photocatalytic activity than ZnO NRs-4-S. With the extension of UV exposure, the intensity of the absorption peak at 664 nm gradually decreases, which indicates that MB is degraded under UV irradiation. The degradation efficiency is defined as $(C_0-C)/C_0$, where C_0 and C are the initial concentration of MB solution and that during the reaction, respectively. After UV irradiation for 1 h, the degradation of MB is only about 3.0% in the absence of any photocatalyst, however, the degradation efficiency of MB is up to 96.8 and 94.1% by employing ZnO NTs-4-N and ZnO NRs-4-S as the photocatalyst, respectively (Fig. 4*d*). The ZnO NTs-4-N shows a little higher degradation efficiency compared with ZnO NRs-4-S, which could attribute to a large surface area [30]. The degradation of MB solution could be considered as a first-order reaction by linear transformation of the following equation [31]

$$-Kt = \ln\left(\frac{C}{C_0}\right) \tag{6}$$

where K is the corresponding degradation rate constant, and t is the reaction time. Fig. 4*e* shows the linear relationship between $\ln(C/C_0)$ and t of photodegradation of MB aqueous solution without or with different photocatalysts, in which the slope is the photodegradation rate constant. The photodegradation rate constants K are calculated to be 0.054 and 0.044 min^{-1} for ZnO NTs-4-N and ZnO NRs-4-S, respectively, which indicates that the photodegradation rate of MB solution with ZnO NTs-4-N is about 1.2 times of that with ZnO NRs-4-S.

The possible photocatalytic mechanism is proposed. At first, the ZnO NTs-4-N and ZnO NRs-4-S absorb photons with energies equal to or larger than their bandgap energies, and generate holes (h^+) in the valence band and electrons (e^-) in the conduction band. The photo-induced electrons react with oxygen (O_2) and holes react with water (H_2O) or hydroxyl groups (OH^-) to generate superoxide radical ($\cdot O_2^-$) and hydroxyl radical (·OH) which are involved in the photocatalytic oxidation reaction. The superoxide radical ($\cdot O_2^-$) could be transformed into hydroxyl radical (·OH)

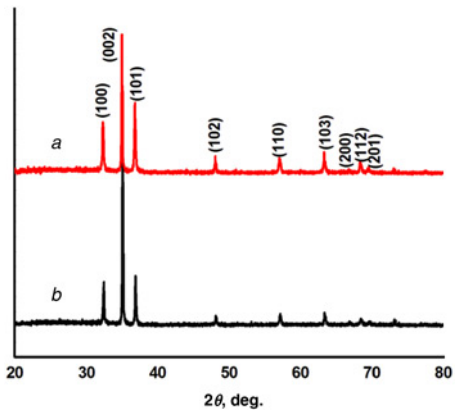

Fig. 3 *XRD of*
a ZnO NTs-4-N
b ZnO NRs-4-S

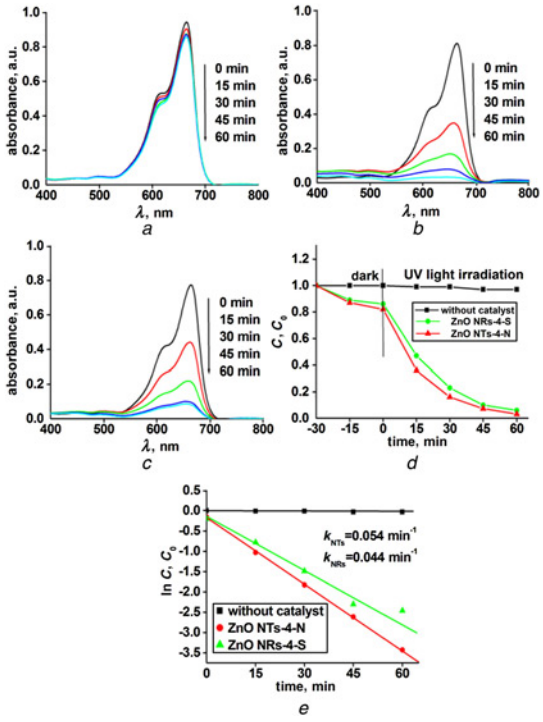

Fig. 4 *Change in the degradation of MB*
a–c The change in the degradation of MB without catalyst, with ZnO NTs-4-N and ZnO NRs-4-S, respectively
d Degradation curves of MB without catalyst and with ZnO NTs-4-N and ZnO NRs-4-S
e First-order plots for the photocatalytic degradation of MB using ZnO NTs-4-N and ZnO NRs-4-S

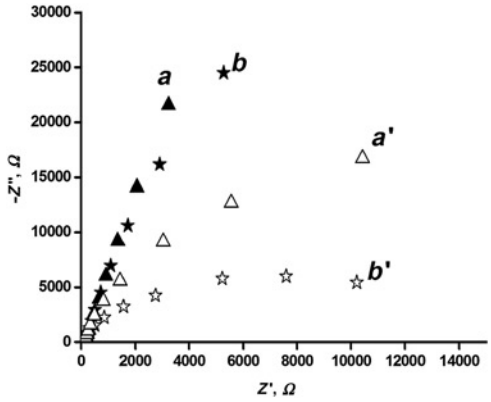

Fig. 5 *EIS response of ZnO NRs-4-S (a, a') and ZnO NTs-4-N (b, b') under UV light irradiation and in dark*

after the multistep reduction [32], which could degrade MB molecules [33].

EIS has been proven to be effective in the investigation of the separation efficiency of electron–hole pairs and the nature of carrier transport processes [34]. The photocatalytic degradation of MB could be explained as an electrochemical oxidation reaction in which reactants supply electrons to an anode. Fig. 5 shows EIS response of ZnO NTs-4-N and ZnO NRs-4-S with and without UV light irradiation ($\lambda = 254$ nm). The radio of the arc on the EIS Nyquist plot reflects the reaction rate occurring on the surface of the electrode and the electrode resistance in the solid-state interface layer. As shown in Fig. 5, the EIS radio of ZnO NTs-4-N electrode is less than that of the ZnO NRs-4-S electrode either under UV irradiation or in dark, which indicates ZnO NTs-4-N possesses smaller charge-transfer resistance and capacitive reactance than ZnO NTs-4-S. That is to say, there is a more effective separation of photo-generated e^-/h^+ pairs and a faster interfacial charge transfer as the photocatalyst is ZnO NTs-4-N. The electron transfer rate from electrolyte to the electrode surface is enhanced in ZnO NTs, which could be attributed to its large specific surface area. The photo-generated electrons could easily flow to the bulk electrode along the longitudinal direction of ZnO NTs that will reduce the probability of e^-/h^+ recombination. Simultaneously, the large number of holes on the surface could promote electron moving to electrode, which will result in an enhancement in the photocatalytic rate. Therefore, both the highly ordered array and large specific surface area could suppress e^-/h^+ recombination, and thereby a highly effective photocatalyst will be achieved [35].

To understand the high photocatalytic performance of ZnO NTs-4-N and ZnO NTs-4-S, their UV–visible diffuse reflectance spectra were also observed. Fig. 6*a* shows that ZnO NTs-4-N and ZnO NTs-4-S both have the weak absorption in the wavelength ranges from visible light to near infrared and the strong absorption at the wavelength <400 nm. It can be seen that the ultraviolet

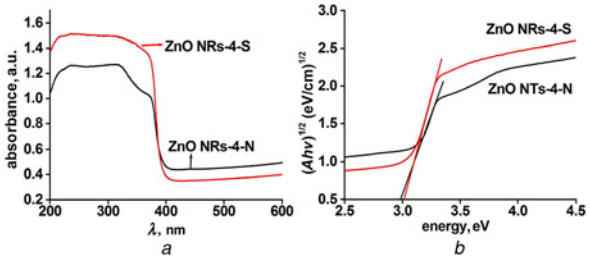

Fig. 6 *UV–visible spectra and plots of $(Ahv)^{1/2}$ against energy (hv) of ZnO NTs-4-N and ZnO NRs-4-S*
a UV–visible spectra
b Plots of $(Ahv)^{1/2}$ against energy (hv)

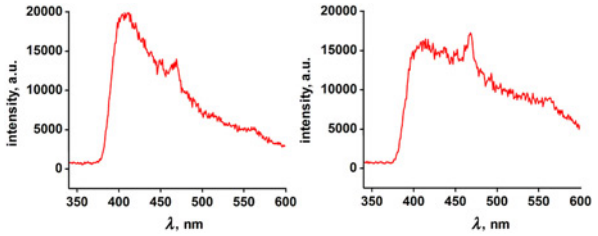

Fig. 7 *PL spectra of ZnO NTs-4-N and ZnO NRs-4-S with 345 nm excitation wavelength*
a PL spectra of ZnO NTs-4-N
b PL spectra of ZnO NRs-4-S

absorption of ZnO NTs-4-N is weaker than that of ZnO NTs-4-S, however, its absorption of visible light is increased. A plot of $(Ahv)^{1/2}$ against energy (hv) shown in Fig. 6*b* is used to estimate the optical bandgap of ZnO nanoarrays, from which the bandgaps of 2.98 eV (ZnO NTs-4-N) and 3.01 eV (ZnO NTs-4-S) could be obtained, respectively. These bandgaps are smaller than the well-known bandgap of 3.37 eV for bulk ZnO. The lower bandgaps make them easier to form photo-induced electrons and holes, which facilitates the electron transfer in the process of photodegradation of dye molecules [14]. As a result, it can be concluded that the lower bandgap of ZnO NTs-4-N in our work contributes to its more effective photocatalytic activity.

PL spectra of ZnO NTs-4-N and ZnO NTs-4-S were surveyed at room temperature with 325 nm excitation wavelength and shown in Fig. 7, which exhibit different features depending on their morphologies. It can be seen that at almost the same position, ZnO NTs-4-N and ZnO NTs-4-S have an UV emission peak (~403 nm) and two blue emission peaks (~450 and 468 nm). However, the relative intensity of UV emission decreases and that of blue emission increases when the morphology changes from NTs to NRs. The UV emission, which corresponds to the near band edge emission, is known to originate from the exciton recombination [36]. Larger specific surface area and smaller bandgap of ZnO NTs-4-N may easily generate photo-induced e^-/h^+ pairs [18, 28]. Therefore, ZnO NTs-4-N shows a stronger emission in 403 nm than ZnO NTs-4-S. The PL result further demonstrates their photocatalytic activity.

4. Conclusion: In conclusion, the well-aligned ZnO nanotubular and nano rod-like arrays were successfully prepared in a controllable mode based on a simple hydrothermal process. The cooling way of hydrothermal synthesis has an important effect on the morphology of nanoarrays. Natural cooling tends to produce nanotubes and the sudden cooling could result in nanorods. The obtained ZnO nanoarrays show excellent photocatalytic activity, especially the ZnO nanotubes because the highly ordered array and large specific surface area could increase the transfer of photo-generated electrons and restrain the recombination of electron–hole pairs. It is reasonable to expect that these well-aligned ZnO nanoarrays proposed in our Letter could be fabricated on different substrates, and will be able to serve as promising photocatalytic material to degrade the organic pollutants in water because of their easily retrievable feature.

5. Acknowledgments: This work was supported by the National Natural Science Foundation of China (grant no. 21201115) and State Key Laboratory of New Ceramic and Fine Processing Tsinghua University (grant no. KF201614).

6 References

[1] Hoffmann M.R., Choi W., Martin S.T.: 'Environmental applications of semiconductor photocatalysis', *Chem. Rev.*, 1995, **195**, pp. 69–96

doi: 10.1049/mnl.2016.0819

[2] Ma L.K., Wang J.N., Wang D.: 'The strategy and policy framework for water pollution control in China during the twelfth five-year plan period', *China Environ. Sci.*, 2013, **33**, pp. 377–383

[3] Zhang L., Wu X., Zheng T., *ET AL.*: 'Green nanotechnology: aqueous photocatalytic degradation of persistent organic pollutants using nanostructured materials', *Nanotechnol. Precis. Eng.*, 2013, **11**, pp. 511–517

[4] Fu D.Y., Han G.Y., Yang F.F., *ET AL.*: 'Seed-mediated synthesis and the photo-degradation activity of ZnO-grapheme hybrids excluding the influence of dye adsorption', *Appl. Surf. Sci.*, 2013, **283**, pp. 654–659

[5] Shao X., Lu W.C., Zhang R., *ET AL.*: 'A comparative study of TiO_2/C hybrid aerogels from $TiCl_4$ or $Ti(OBu)_4$ for photocatalytic methylene blue degradation', *New Carbon Mater.*, 2013, **28**, pp. 378–384

[6] Qin Y., Wang X.D., Wang Z.L.: 'Microfiber nanowire hybrid structure for energy scavenging', *Nature*, 2008, **451**, pp. 809–813

[7] Jing L., Wang D., Wang B., *ET AL.*: 'Effects of noble metal modification on surface oxygen composition, charge separation and photocatalytic activity of ZnO nanoparticles', *J. Mol. Catal.*, 2006, **A244**, pp. 193–200

[8] Wang S.W., Yu Y., Zuo Y.H., *ET AL.*: 'Synthesis and photocatalysis of Hierarchical hetero assemblies of ZnO branched nanorod arrays on Ag core nanowires', *Nanoscale*, 2012, **4**, pp. 5895–5901

[9] Xia W.W., Mei C., Zeng X., *ET AL.*: 'Nanoplate-built ZnO hollow microspheres decorated with gold nanoparticles and their enhanced photocatalytic and gas-sensing properties', *ACS Appl. Mater. Interfaces*, 2015, **7**, pp. 11824–11832

[10] Han J., Shi L.Y., Cheng R.M., *ET AL.*: 'Silver modified ZnO thin films and their photocatalytic activity', *Chin. J. Inorg. Chem.*, 2008, **24**, pp. 950–955

[11] Kim H., Jeong H., An T.K., *ET AL.*: 'A hybrid-type quantum-dot cosensitized ZnO nanowire solar cell with enhanced visible-light harvesting', *ACS Appl. Mater. Interfaces*, 2013, **5**, pp. 268–275

[12] Yang J.L., An S.J., Park W.I., *ET AL.*: 'Photocatalysis using ZnO thin films and nanoneedles grown by metal organic chemical vapor deposition', *Adv. Mater.*, 2004, **16**, pp. 1661–1664

[13] Saoud K., Alsoubaihi R., Bensalah N., *ET AL.*: 'Synthesis of supported silver nano-spheres on zinc oxide nanorods for visible light photocatalytic applications', *Mater. Res. Bull.*, 2015, **63**, pp. 134–140

[14] Bae J., Han J.B., Zhang X.M., *ET AL.*: 'ZnO nanotubes grown at low temperature using Ga as catalysts and their enhanced photocatalytic activities', *J. Phys. Chem. C*, 2009, **113**, pp. 10379–10383

[15] Fu D.Y., Han G.Y., Chang Y.Z., *ET AL.*: 'The synthesis and properties of ZnO–graphene nano hybrid for photodegradation of organic pollutant in water', *Mater. Chem. Phys.*, 2012, **132**, pp. 673–681

[16] Ma L., Ai X., Huang X., *ET AL.*: 'Effects of the substrate and oxygen partial pressure on the microstructures and optical properties of Ti-doped ZnO thin films', *Superlattice Microstruct.*, 2011, **50**, pp. 703–712

[17] Serpone N., Lawless D., Khairutdinov R.: 'Size effects on the photophysical properties of colloidal anatase TiO_2 particles: size quantization versus direct transitions in this indirect semiconductor', *J. Phys. Chem.*, 1995, **99**, pp. 16646–16654

[18] Li D., Shi R., Pan C.S., *ET AL.*: 'Influence of $ZnWO_4$ nanorod aspect ratio on the photocatalytic activity', *CrystEngComm*, 2011, **13**, pp. 4695–4700

[19] Kuo T.J., Lin C.N., Kuo C.L., *ET AL.*: 'Growth of ultralong ZnO nanowires on silicon substrates by vapor transport and their use as recyclable photocatalysts', *Chem. Mater.*, 2007, **19**, pp. 5143–5147

[20] Sun T.J., Qiu J.S., Liang C.H.: 'Controllable fabrication and photocatalytic activity of ZnO nanobelt arrays', *J. Phys. Chem. C*, 2008, **112**, pp. 715–721

[21] Wang J., Zhuang H.Z., Xue C.S., *ET AL.*: 'Structure and formation mechanism of Sn-doped ZnO nanoneedles', *Acta Phys.-Chim. Sin.*, 2010, **26**, pp. 2840–2844

[22] Yoshida T., Tachibana T., Maemoto T., *ET AL.*: 'Pulsed laser deposition of ZnO grown on glass substrates for realizing high-performance thin-film transistors', *Appl. Phys. A*, 2010, **101**, pp. 685–688

[23] Fu D.Y., Han G.Y., Meng C.F.: 'Size-controlled synthesis and photocatalytic degradation properties of nano-sized ZnO nanorods', *Mater. Lett.*, 2012, **72**, pp. 53–56

[24] Saravanan R., Kumar G.V., Narayanan V., *ET AL.*: 'Comparative study on photocatalytic activity of ZnO prepared by different methods', *J. Mol. Liq.*, 2013, **181**, pp. 133–141

[25] Zheng J.H., Zhang X.K., Lu H.F.: 'Synthesis and characterization of well-aligned ZnO nanorod arrays under specific conditions', *Acta Chim. Sin.*, 2011, **69**, pp. 2434–2438

[26] Dong J.T., Zhang F.C., Zhang W.H., *ET AL.*: 'Hydrothermal fabrication and optical properties of ZnO nanorods', *Semicond. Sci. Technol.*, 2011, **36**, pp. 657–660

[27] Liu Z.F., Liu C.C., Ya J., *ET AL.*: 'Controlled synthesis of ZnO and TiO_2 nanotubes by chemical method and their application in dye-sensitized solar cells', *Renew. Energy*, 2011, **36**, pp. 1177–1181

[28] Roza L., Rahman M.Y.A., Umar A.A., *ET AL.*: 'Direct growth of oriented ZnO nanotubes by self-selective etching at lower temperature for photo-electrochemical (PEC) solar cell application', *J. Alloys Compd.*, 2015, **618**, pp. 153–158

[29] Xi Y., Wu W.Z., Fang H., *ET AL.*: 'Integrated ZnO nanotube arrays as efficient dye-sensitized solar cells', *J. Alloys Compd.*, 2012, **529**, pp. 163–168

[30] Chen D.M., Wang Z.H., Ren T.Z., *ET AL.*: 'Influence of defects on the photocatalytic activity of ZnO', *J. Phys. Chem. C*, 2014, **118**, pp. 15300–15307

[31] McLaren A., Solis T.V., Li G.Q., *ET AL.*: 'Shape and size effects of ZnO nanocrystals on photocatalytic activity', *J. Am. Chem. Soc.*, 2009, **131**, pp. 12540–12541

[32] Kang Z.H., Tsang C.H.A., Wong N.B., *ET AL.*: 'Silicon quantum dots: a general photocatalyst for reduction, decomposition, and selective oxidation reactions', *J. Am. Chem. Soc.*, 2007, **129**, pp. 12090–12091

[33] Pan C.S., Zhu Y.F.: 'New type of $BiPO_4$ oxy-acid salt photocatalyst with high photocatalytic activity on degradation of dye', *Environ. Sci. Technol.*, 2010, **44**, pp. 5570–5574

[34] Liu H., Cheng S.A., Wu M., *ET AL.*: 'Photoelectrocatalytic degradation of sulfosalicylic acid and its electrochemical impedance spectroscopy investigation', *J. Phys. Chem. A*, 2000, **104**, pp. 7016–7020

[35] Sun L., Cai J.H., Wu Q., *ET AL.*: 'N-doped TiO_2 nanotube array photoelectrode for visible-light-induced photoelectrochemical and photoelectrocatalytic activities', *Electrochim. Acta*, 2013, **108**, pp. 525–531

[36] Zuo H.F., Guo Y.R., Li S.J., *ET AL.*: 'Application of microcrystalline cellulose to fabricate ZnO with enhanced photocatalytic activity', *J. Alloys Compd.*, 2014, **617**, pp. 823–827